Fuel 333 (2023) 126533

Contents lists available at ScienceDirect

Fuel

journal homepage: www.elsevier.com/locate/fuel

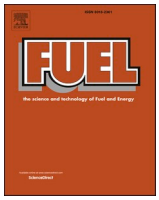

Comparing different syngas for blast furnace ironmaking by using the extended operating line methodology

Manuel Bailera [a,b,*]

[a] Graduate School of Creative Science and Engineering, Waseda University, Okubo, Shinjuku-ku, Tokyo 169-8555, Japan
[b] Escuela de Ingeniería y Arquitectura. Universidad de Zaragoza, Campus Río Ebro, María de Luna 3, 50018 Zaragoza, Spain

ARTICLE INFO

Keywords:
Syngas
Ironmaking
Blast furnace
Operating diagram
Extended operating line

ABSTRACT

This paper assesses the injection of different syngas in air-blown blast furnaces, oxygen blast furnaces, and advanced oxygen blast furnaces. The selected types of syngas come from biomass gasification, plastic gasification, CO_2 electrolysis, and reverse water–gas shift reaction. An Aspen Plus model, based on the new extended operating line methodology, was used for the simulation. This methodology is a generalization of the conventional Rist diagram, to extend its application to cases in which the injected gases have large contents of CO_2 and H_2O, and also to cases in which injections take place at the middle or upper zone of the blast furnace. The base cases were elaborated and validated with data from literature, with a discrepancy below 3.5%. A total of 7 key performance indicators were defined for the study (mass flow of syngas, coke replacement ratio, gas utilization, percentage of direct reduction, blast furnace gas temperature, flame temperature, and net CO_2 emissions). In practice, the amount of syngas that can be injected is limited to 92 – 264 kg_{syngas}/tHM because of the drop in the flame temperature. The lowest net CO_2 emissions are achieved in oxygen blast furnace with injection of syngas from reverse water–gas shift reaction.

1. Introduction

The iron and steel industry is one of the major carbon emitter industries in the world [1]. It is the second largest consumer of industrial energy (7200 TWh/y) [2], and responsible of 9 % of the total CO_2 emissions worldwide (3.7 Gt_{CO2}/y) [1,3]. Currently, the main manufacturing process for the production of iron is the blast furnace (BF) technology [4,5]. In blast furnaces, iron ore and coke are introduced at the top. The iron oxide is reduced (Eq. (1) and Eq. (2)) while descending thanks to a reducing gas that ascends in counter-current [6]. This gas is produced at the lower part of the furnace by burning the coke with O_2-enriched air that is injected through the tuyeres. Auxiliary fuels, such as pulverized coal or natural gas can be also injected through the tuyeres to decrease the coke input [7].

$$Fe_2O_3 + 3CO \rightarrow 2Fe + 3CO_2 \quad (1)$$

$$Fe_2O_3 + 3H_2 \rightarrow 2Fe + 3H_2O \quad (2)$$

Because of the requirement of high-temperature heat (above 800–1200 °C) and the nature of the process itself (CO_2 release during reduction), the blast furnace ironmaking process cannot be decarbonized with electrification [8]. Within this framework, some authors have studied the utilization of syngas and renewable fuels in the blast furnace [8–10]. Syngas is a CO_2-neutral fuel gas that is synthetically obtained and is commonly constituted of carbon monoxide, hydrogen and carbon dioxide (the CO_2-neutrality extent will depend on the raw material used for the syngas production). Its components make syngas a useful resource in ironmaking as a reducing agent for the blast furnace. This can be injected through the tuyeres to substitute part of the coke that is introduced with the burden, or to replace other auxiliary fuels [11].

One of the main sources of syngas is biomass [12]. However, the utilization of biomass in ironmaking is traditionally proposed in literature as pulverized solid fuel (charcoal obtained by pyrolysis) [13–16], rather than as syngas. Only Babich et al. [17] studied the injection of syngas, who proposed it as a method for increasing the efficiency of biomass usage. During pyrolysis, liquid and gaseous fuels are also produced, so its utilization as auxiliary reducing agents would rise the economic efficiency of using charcoal in the steel plant (Fig. 1). They calculated coke reductions of 19.3 kg/THM when injecting 36.2 kg/THM of pyrolysis biogas at 1200 °C (0.5 kg_{coke}/kg_{syngas} replacement ratio), and coke reductions of 13.6 kg/tHM when injecting 44.4 kg of syngas (0.3 kg_{coke}/kg_{syngas} replacement ratio).

* Author at: Escuela de Ingeniería y Arquitectura. Universidad de Zaragoza, Campus Río Ebro, María de Luna 3, 50018 Zaragoza, Spain.
E-mail address: mbailera@unizar.es.

https://doi.org/10.1016/j.fuel.2022.126533
Received 18 May 2022; Received in revised form 7 September 2022; Accepted 26 October 2022
Available online 7 November 2022
0016-2361/© 2022 The Author(s). Published by Elsevier Ltd. This is an open access article under the CC BY-NC license (http://creativecommons.org/licenses/by-nc/4.0/).

Nomenclature

Acronyms

AdOBF	advanced oxygen blast furnace
BF	blast furnace (air-blown, unless otherwise specified)
BFG	blast furnace gas
CC	carbon capture
EX	heat exchanger
HM	hot metal
KPI	key performance indicator
OBF	oxygen blast furnace
pp	percentage points
RWGS	reverse water–gas shift
SOEC	solid oxide electrolytic cell

Symbols

A	calculation parameter, kcal/mol
a_j	number of moles of H_2 in injectant j per number of moles of injectant j, -
B	calculation parameter, kcal/mol
b_j	number of moles of O_2 in injectant j per number of moles of injectant j, -
C	calculation parameter, kcal/mol
$C_{\Delta T_R}$	sensible heat of the burden between $T_R - \Delta T_R$ and T_R (lack of thermal ideality), kcal/mol_{Fe}
D	calculation parameter, -
E	calculation parameter, -
e	number of moles of H_2O per number of atoms of O in the air (i.e., $e = y_e/y_v$), -
F	calculation parameter, -
f	sensible heat of the hot metal between T_R and T_f (outlet temperature), kcal/mol_{Fe}
l	sensible heat of the slag between T_R and T_l (outlet temperature), kcal/mol_{Fe}
M	molar weight, kg/kmol
m	mass flow, kg/t_{HM}
n	mole flow, kmol/t_{HM}
p	heat removed by the staves in the elaboration zone, kcal/mol_{Fe}
q_c	heat released at T_R by the reaction$C\ (coke) + 0.5\ O_2 \rightarrow CO$, kcal/$mol_O$
q_e	heat required by the H_2O in hot blast due to dissociation, reverse water–gas shift and sensible heat, kcal/mol_{H2O}
q_g	heat absorbed at T_R by the reaction $C + CO_2 \rightarrow 2CO$, kcal/mol_C
q_j	thermal demand by injectant j, $CH_{2a}O_{2b}N_{2c}S_{2d}Z_z$ (or $H_{2a}O_{2b}N_{2c}$ or $O_{2b}N_{2c}$) due to dissociation, sensible heat, reverse water–gas shift of the H_2, incomplete combustion with the O_2, and transfer of S to the slag, kcal/mol_j
q_k	heat absorbed at T_R by the total H_2 in the furnace when considering that it is completely converted to H_2O through the reverse water–gas shift reaction, kcal/mol_{H2}
q_{mid}	energy consumption to heat the shaft injection to T_R, kcal/mol_{mid}
q_{Mn}	heat absorbed at T_R by the reaction $C + MnO \rightarrow CO + Mn$, kcal/$mol_O$
q_P	heat absorbed at T_R by the reaction$1/5 P_2O_5 \cdot 3CaO + C + 6/5 Fe \rightarrow 2/5 Fe_3P + 3/5 CaO + CO$, kcal/$mol_O$
q_{Si}	heat absorbed at T_R by the reaction$C + 1/2\ SiO_2 + 3/2\ Fe \rightarrow CO + 1/2\ Fe_3Si$, kcal/$mol_O$
q_v	energy available from the sensible heat of the air between T_v and T_R, kcal/mol_O
q_γ	heat absorbed at T_R by the carburization of the iron, kcal/mol_C
r	chemical efficiency of the blast furnace, -
T	temperature, K (unless otherwise specified)
X	abscissa in the extended diagram, -
$x_{CO2,j}$	number of moles of CO_2 entering with injectant j, per mole of BFG (excl. N_2), -
x_d	number of moles of CO that have received an O removed from wüstite by direct reduction, per mole of BFG (excl. N_2), -
x_e	number of moles of H_2O in hot blast, per mole of BFG (excl. N_2), -
x_h	molar fraction of hydrogen and water in gas mixture, -
$x_{H2O,j}$	number of moles of H_2O entering with injectant j, per mole of BFG (excl. N_2), -
x_i	number of moles of O atoms removed from burden by indirect reduction, per mole of BFG (excl. N_2), mol_O/mol_{BFG}
x_j	number of moles of injectant j, per mole of BFG (excl. N_2), -
x_k	number of moles of H_2 in the coke, per mole of BFG (excl. N_2), -
x_{mb}	number of moles of moisture in the burden, per mole of BFG (excl. N_2), -
x_{mid}	number of moles of injection in the mid zone, per mole of BFG (excl. N_2), -
x_{Mn}	number of moles of CO produced via the direct reduction of MnO, per mole of BFG (excl. N_2), -
x_P	number of moles of CO produced via the direct reduction of P_2O_5, per mole of BFG (excl. N_2), -
x_S	number of moles of CO produced via the transfer of S to the slag, per mole of BFG (excl. N_2), -
x_{Si}	number of moles of CO produced via the direct reduction of SiO_2, per mole of BFG (excl. N_2), -
x_{up}	number of moles of injection in the preparation zone, per mole of BFG (excl. N_2), -
x_v	number of moles of CO produced by the O_2 of the hot blast via the combustion of C, per mole of BFG (excl. N_2), -
Y	ordinate in the extended diagram, -
$y_{CO2,j}$	number of moles of CO_2 entering with injectant j, per mole of Fe produced, -
y_d	number of moles of CO that have received an O removed from wüstite by direct reduction, per mol of Fe produced, -
y_e	number of moles of H_2O in hot blast, per mole of Fe produced, -
Y_E	intercept of the extended operating line (moles of blast furnace gas that have not received any O coming from the iron oxides through the direct reduction process, per mole of Fe produced; negative sign by convention), -
Y_E^*	terms of Y_E that are independent of y_v, -
$y_{H2O,j}$	number of moles of H_2O entering with injectant j, per mole of Fe produced, -
y_i	number of moles of O transferred from the iron oxides to the gas by indirect reduction per mol of Fe produced, -
y_j	number of moles of injectant j, per mole of Fe produced, -
y_k	number of moles of H_2 in the coke, per mole of Fe produced, -
y_{mb}	number of moles of moisture in the burden, per mole of Fe produced, -
y_{mid}	number of moles of injection in the mid zone, per mole of Fe produced, -
y_{Mn}	number of moles of CO produced via the direct reduction of MnO, per mole of Fe produced, -
y_P	number of moles of CO produced via the direct reduction of P_2O_5, per mole of Fe produced, -
y_S	number of moles of CO produced via the transfer of S to the slag, per mole of Fe produced, -
y_{Si}	number of moles of CO produced via the direct reduction of

	SiO_2, per mole of Fe produced, -
y_{up}	number of moles of injection in the preparation zone, per mole of Fe produced, -
y_v	number of moles of CO produced by the O_2 of the hot blast via the combustion of C, per mole of Fe produced, -

Greek symbols

μ	slope of the extended operating line (total number of moles of blast furnace gas, without accounting N_2, per 1 mol of Fe produced), -
η_{CO,H_2}	reducing gas utilization factor, defined as the percentage of reducing species that are oxidized in the final blast furnace gas, i.e.,$\eta_{CO,H_2} = 100\cdot(n_{H2O}+n_{CO2})/(n_{CO}+n_{CO2}+n_{H2}+n_{H2O})$, %
τ_j	calculation parameter that is 1 when the auxiliary injection j contains carbon and 0 when not, -
ω	molar fraction or oxidation state, -
$\Omega_{j,i}$	mass fraction of compound i in stream j, -

Subscripts and superscripts

A	initial oxidation state of the iron oxides at the inlet of the blast furnace
BFG*	blast furnace gas that exits the system (i.e., that is not recirculated to the BF or to the CC stage)
CC	carbon capture
F	projection of the coordinates of the equilibrium with wüstite
f	hot metal
fl	flame
k	coke
l	slag
M	coordinates of the equilibrium with magnetite
OC	related to the equilibrium of CO and CO_2 with pure wüstite
OH	related to the equilibrium of H_2 and H_2O with pure wüstite
OHC	related to the equilibrium of CO, CO_2, H_2 and H_2O with pure wüstite
P	characteristic point of the extended operating line related to the energy balance of the elaboration zone
R	characteristic point of the extended operating line referring to the thermal reserve zone
Syn	syngas
W	coordinates of the equilibrium with wüstite

Non-steel sectors, such as plastic consumers, are also an important sources of syngas for iron-making (in this case, the syngas would not be CO_2-neutral). As occurred in the case of biomass, the utilization of waste plastic in ironmaking has been usually proposed in literature as a pulverized solid fuel injection [19–21], instead of as syngas injection. Nevertheless, waste plastic can be gasified to generate syngas and partially substitute coke and pulverized coal. A recent study revealed that the syngas coming from gasified plastics can substitute about 18 kg/THM of coke per 99.3 kg/tHM of syngas (0.18 kg_{coke}/kg_{syngas} replacement ratio) [22].

Syngas can also be produced through Power to Gas technology, which uses renewable electricity to obtain combustible gases by electrolysis [23]. The technology is ready for energy storage (Audi's PtG plant was qualified for participating in the German electricity balancing market) [24], although it needs subsidies to be profitable [25]. Its application to industries has been proved to be a more cost-effective solution [26,27]. In ironmaking, the CO_2 that is emitted can be electrolyzed to directly produce synthesis gas (CO_2 electrolysis), or alternatively, water can be electrolyzed to obtain H_2 which, in combination with CO_2, is then used to produce synthesis gas through the reverse water–gas shift (RWGS) reaction (Fig. 1) [28]. In both cases, the carbon is continuously recycled by producing syngas from the CO_2 released in the blast furnace.

Currently, the only CO_2 electrolysis process solution near commercialization that has proven its reliability over the long term is the high-temperature solid oxide electrolytic cell (SOEC). The SOEC can use the blast furnace gas (BFG) as such or just its CO_2 content after a CO_2 stripping stage. Moreover, the CO_2 electrolysis by-produces O_2 that can be used in the blast furnace to enrich the air and diminish the electricity consumption of the air separation unit [29]. Different studies have explored this integration, suggesting that CO_2 emission cuts of 11–22 % are possible, at specific electrical consumptions of 4.8 – 10.8 MJ/kg_{CO2} and specific thermal consumptions of 1.0 – 2.5 MJ/kg_{CO2} [29]. Regarding the production of syngas through the RWGS reaction, it presents similar energy consumptions as the CO_2 electrolysis route, according to the study of Kato [30] (4.9 MJ/kg_{CO2} electrical consumption, and 2.0 MJt/kg_{CO2} thermal consumption).

The utilization of the different types of syngas has not been compared in literature under the same framework. Thus, the first novelty of the present paper is to characterize and compare the utilization of different syngas under the same blast furnace configuration. Additionally, the second novelty of the paper is to perform this study not only under air-blown blast furnaces, but also for oxygen blast furnaces [31], and advanced oxygen blast furnaces [32]. The utilization of syngas has not been evaluated so far in literature for the two latter types of blast furnaces. In order to do that, the extended operating line methodology is used [33]. This methodology is a recently proposed generalization of the conventional Rist diagram, to extend its application to cases in which the injected gases have large contents of CO_2 and H_2O, and also to cases in which injections take place at the middle or upper zone of the blast furnace. Therefore, the third novelty of the paper is the application of this new methodology to the assessment of the performance of syngas in blast furnaces.

2. Definition of case studies and key performance indicators

Four type of syngas were selected for the comparison study, covering syngas from biomass gasification, syngas from waste plastic gasification, syngas from CO_2 electrolysis, and syngas from the reverse water–gas shift reaction (Table 1). The different syngas injections are assumed to take place at 900 °C [31], at the tuyeres, and the results were compared with the corresponding base case in which no syngas is injected.

The four types of syngas were assessed at three types of blast furnaces: air-blown blast furnaces, oxygen blast furnaces (OBF), and advances oxygen blast furnaces (AdOBF) (Fig. 2). The air-blown BF reproduces the data from Babich et al. [17], characterized by 0.92 chemical efficiency, 850 °C thermal reserve zone temperature, 701.1 MJ/tHM heat losses, and 31 % H_2 utilization. The discrepancy between the results of the extended operating line model and the reference data is below 3.5 % (validation was presented in [33]). To have a fair comparison, these results were taken as basis for the elaboration of the OBF and AdOBF base cases, including modifications in the operating parameters when necessary in agreement with literature.

In oxygen blast furnaces, pure oxygen is used in the combustion instead of air, at the lower part of the furnace. To control the flame temperature, part of the blast furnace gas is recirculated, after passing through a carbon capture stage (in the present study, 90 % of the CO_2 and 100 % of the H_2O were rejected in this stage) [32]. In this case, 60 % of the recirculated gas was injected at the middle zone at 1000 °C, and 40 % at the tuyeres at 25 °C [31,32]. The amount of BFG diverted to the capture stage was set in order to keep a similar flame temperature as in the air-blown BF case (around 2400 °C). This meant injecting a total of

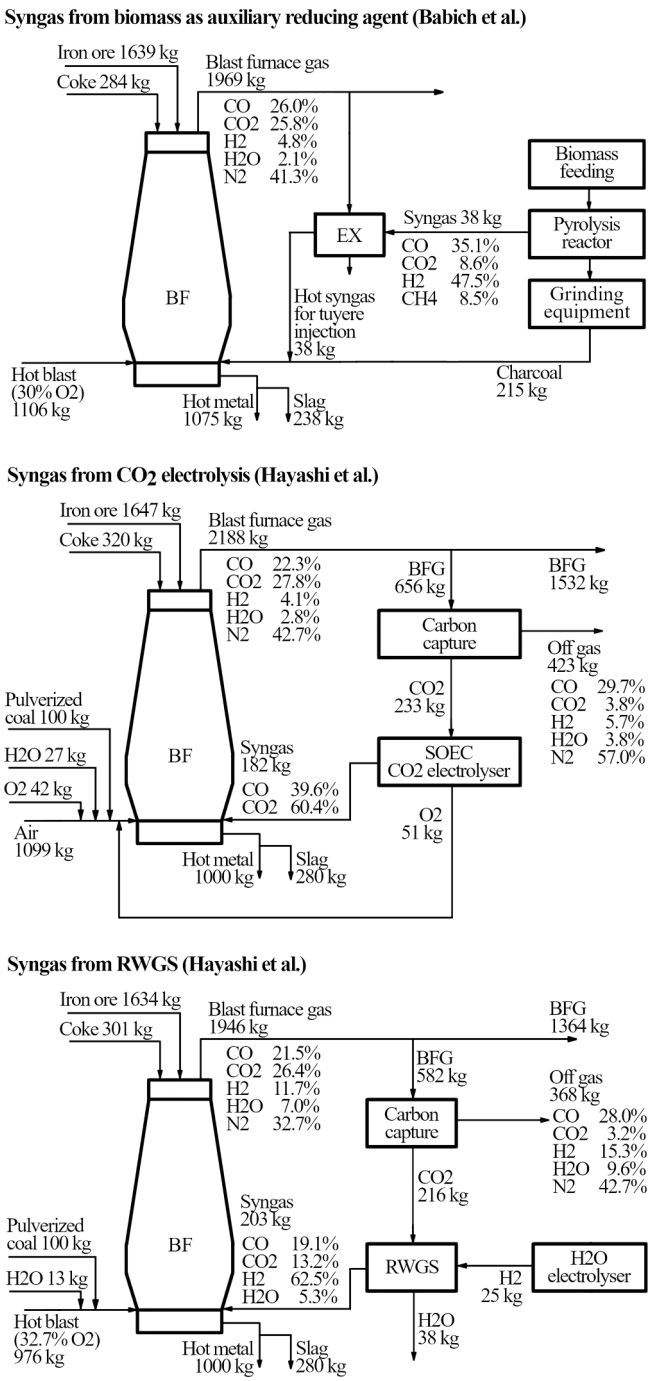

Fig. 1. Process flow diagrams of the integrations of syngas in ironmaking found in literature (data from [17,18]).

Table 1
Molar composition (vol%) of syngas depending on the source [17,18,29,34].

	Biomass gasification	Plastic gasification	CO_2 electrolysis	RWGS
CO	37	23	60	19
CO_2	10	28	40	13
CH_4	0	15	0	0
H_2	36	34	0	63
H_2O	4	0	0	5
N_2	13	0	0	0

640 Nm^3 of CO and H_2 into the blast furnace, accounting for both the shaft and tuyere recirculation (this amount of recirculated reducing gas was kept constant for all the assessments of syngas injection). The chemical efficiency was increased to 0.94 [32], the thermal reserve zone temperature was increased to 950 °C [31], the heat losses were diminished to 500 MJ/tHM [35], and the H_2 utilization was kept constant at 31 %. Lastly, the pulverized coal input was decreased to 170 kg/tHM [31], in order to have a reasonable amount of coke input.

In advanced oxygen blast furnaces, methane is injected at the tuyeres to control the flame temperature, instead of recirculated gas [32]. This causes a lack of thermal energy in the upper part of the furnace, which is palliated by burning some BFG with pure oxygen, and injecting the resulting gas. This gas must be injected above the chemical reserve zone, aiming to preheat the solids entering at the top (it does not matter that the gas is mainly composed by CO_2 and H_2O, since the objective is providing heat, not reducing the iron oxides). The AdOBF has the advantage of avoiding the carbon capture stage. In the present study, the amount of methane injected at the tuyeres was 75 kg/tHM, to keep a similar flame temperature as in the air-blown BF case (around 2400 °C). The upper injection was fixed at 200 Nm^3/tHM, at 1000 °C [32]. The chemical efficiency was set to 0.94 [32], the thermal reserve zone temperature was 950 °C [32], the heat losses were diminished to 250 MJ/tHM [32], and the H_2 utilization was increased to 60 % because of the injection of H_2O at the upper zone. Lastly, the pulverized coal input was kept at 200 kg/tHM, as in the air-blown blast furnace [17].

Thus, there are a total of 12 study cases (4 types of syngas × 3 types of blast furnace), which were compared with each other and with their corresponding base case (in which no syngas injection is considered). To assess these scenarios, 7 key performance indicators (KPI) were defined. The KPIs quantify the most significant aspects that may have an impact on the overall system performance (Table 2). These KPIs allow establishing the maximum syngas injection rate, and compare the net CO_2 emissions of each configuration. The most restrictive KPI is the flame temperature drop when syngas is injected into the blast furnace, since it should not fall below 2000 °C according to literature [7]. Regarding the net CO_2 emissions (Eq. (3)), they are computed as the total CO_2-equivalent emissions exiting the system (i.e., the CO_2-equivalent from the BFG not recirculated, plus the CO_2 from amine scrubbing; see Fig. 2) minus the contribution of the syngas injection. The CH_4, CO and CO_2 content of the syngas ends up in the BFG in the form of CO and CO_2, but this content is considered CO_2-neutral (except for plastic-based syngas), hence they are subtracted in Eq. (3). It must be noted that the concept of CO_2-equivalent emissions assumes that the CO and CH_4 content of the gases will end up as CO_2 after combustion.

$$KPI_7 = \left(\left(n_{BFG^*,CO_2} + n_{BFG^*,CO} + n_{CC,CO_2}\right) - \left(n_{Syn,CO_2} + n_{Syn,CO} + n_{Syn,CH_4}\right)\right) M_{CO2} \quad (3)$$

It is worth to mention that performance of the different BF will differ even if no syngas is injected, mainly because of the inherent characteristics of each configuration. It is reasonable that novel proposals give better performance, since they are intended for improving conventional technologies (in terms of efficiency, CO_2 emissions, raw material consumption, etc.). Therefore, the present paper will show these differences between technologies, and also how the different syngas change the characteristic performance of every type of BF configuration.

3. Methodology

3.1. Extended operating line methodology

The extended operating line (Fig. 3) [33] was used for the modelling of the blast furnace, which is a convenient methodology for predicting changes when the operating conditions are modified. The full calculation methodology was proposed and thoroughly described by Bailera et al. in 2022 [33], which is a generalization of the operating line

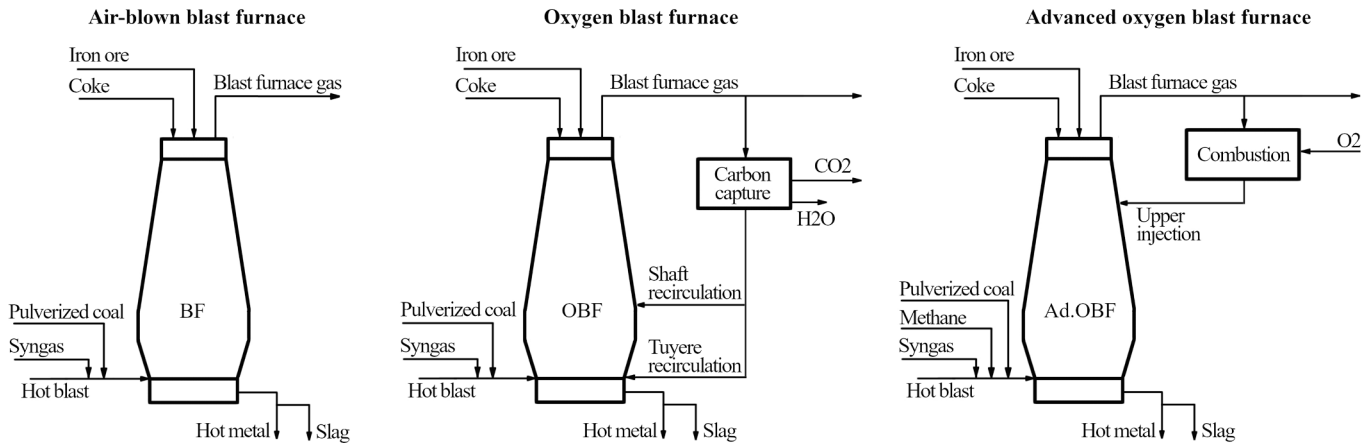

Fig. 2. Conceptual diagrams of air-blown blast furnaces, oxygen blast furnaces, and advanced oxygen blast furnaces, with syngas injection at the tuyeres.

Table 2
Key performance indicators for assessing the syngas injection in blast furnaces.

KPI	Description	Units
KPI_1	Mass flow of syngas injected to the blast furnace	kg/t_{HM}
KPI_2	Coke replacement ratio	kg_{coke}/kg_{syngas}
KPI_3	Gas utilization, η_{CO-H2}	%
KPI_4	Percentage of direct reduction in the blast furnace	%
KPI_5	BFG Temperature, T_{BFG}	°C
KPI_6	Flame temperature, T_{fl}	°C
KPI_7	Net CO_2 emissions	kg/t_{HM}

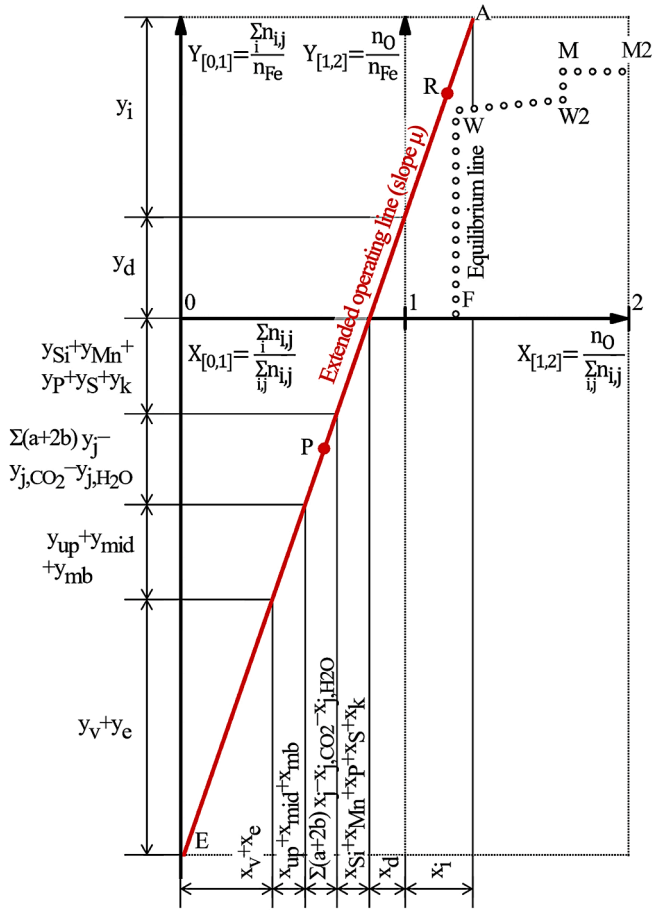

Fig. 3. Extended operating line.

proposed by Rist in 1967 [36,37]. Conventional Rist models are constructed by assuming (i) constant ratio along the blast furnace between the moles of reducing gas and the moles of Fe produced, and (ii) absence of oxidized gases at the beginning of the indirect reduction process. However, the first assumption is not met when injecting gases in the shaft or preheating zone, and the second assumption is not fulfilled when the synthetic gases have CO_2 or H_2O contents. For these reasons, conventional Rist diagrams are not valid when aiming for evaluating the new blast furnace decarbonization concepts presented in this manuscript. Hence, the extended methodology is considered [33], which can deal with gas injections at any part of the blast furnace (i.e., no constant mole flow along the BF), and with gas injections that already contain oxidized components (i.e., a non-continuous oxidation profile during the gas ascent). It should be noted that this methodology has been recently developed, and no other study in literature has used it for assessing syngas injections in blast furnaces.

The extended operating line of a blast furnace is the graphical representation of the mass and energy balances concerning the formation of the blast furnace gas (range $0 < X < 1$ in a Cartesian plot) and the transfer of oxygen from the iron ore to the gas (range $1 < X < 2$ of the plot). The equation of the operating line can be written as Eq. (4). The slope, μ, is the total number of moles of blast furnace gas (without accounting N_2) per 1 mol of Fe produced. The intercept, Y_E, represents the moles of blast furnace gas that have not received any O coming from the iron oxides through the direct reduction process, per mole of Fe produced [38].

$$Y = \mu \cdot X + Y_E \tag{4}$$

In practice, the slope and the intercept are calculated from the coordinates of two characteristic points denoted by P and R (Eq. (5) and Eq. (6)). The point P is imposed by the energy balance of the blast furnace, while the point R represents the equilibrium reached in the middle zone between gases and solids according to the phase diagram.

$$\mu = \frac{Y_R - Y_P}{X_R - X_P} \tag{5}$$

$$Y_E = Y_R - X_R\left(\frac{Y_R - Y_P}{X_R - X_P}\right) \tag{6}$$

The coordinates of the point P are given by Eq. (7) and Eq. (8), where A, B, C and Y_E^* are given by Eqs. (9)–(12).

$$Y_P = Y_E^* - \left(\frac{C}{B} + Y_E^*\right)\left(\frac{B(1+2e)}{A+B(1+2e)}\right) \tag{7}$$

$$X_P = \frac{B(1+2e)}{A+B(1+2e)} \tag{8}$$

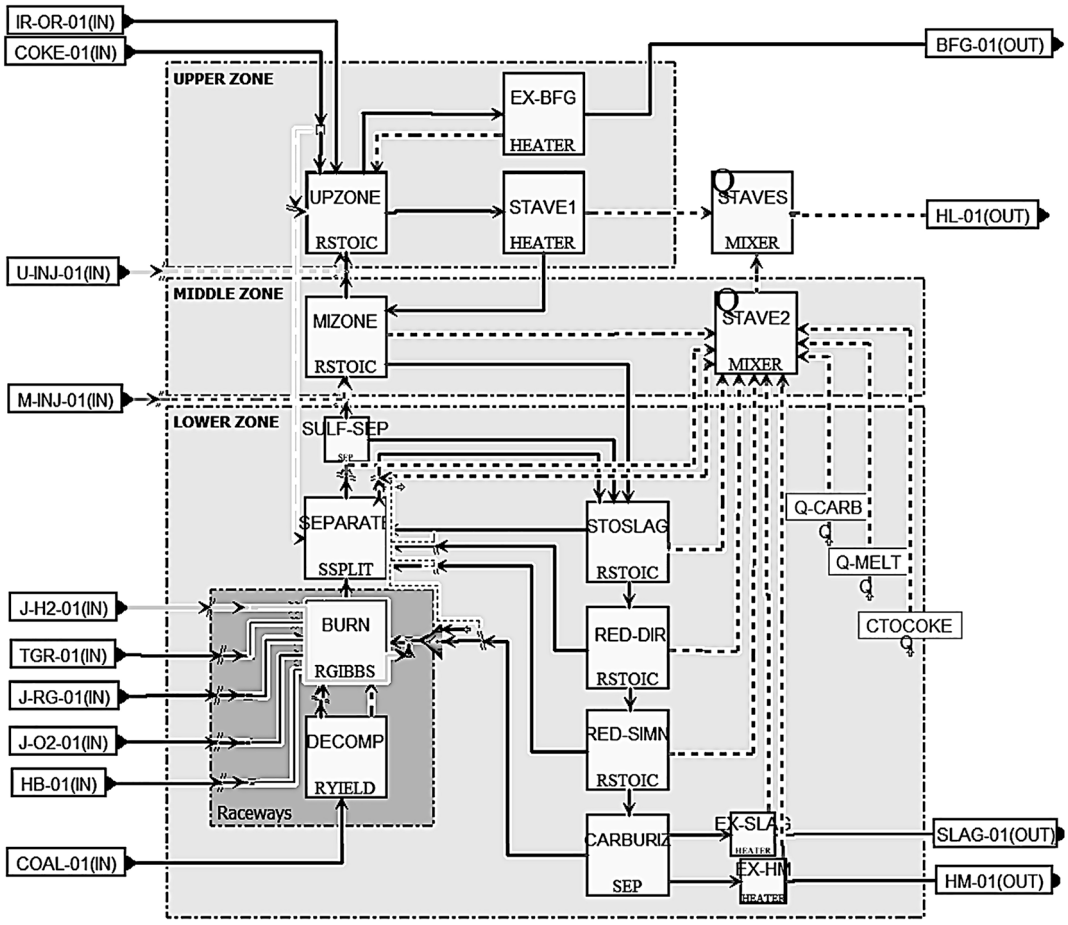

Fig. 4. Process flow diagram of the blast furnace in Aspen Plus.

$$A = q_c + q_v - eq_e + eq_k(1-r) + eq_g \tag{9}$$

$$B = q_g \tag{10}$$

$$C = -q_{iw}Y_w + \delta + q_k y_k + \sum q_j y_j - (1-r)\left(y_k + \sum a_j y_j\right)q_k + q_{Si}y_{Si} + q_{Mn}y_{Mn} + q_P y_P + q_\gamma \gamma + f + l + p + C_{\Delta T_R} - q_g\left(y_{CO2,j} + y_{H2O,j}\right) + q_{mid}y_{mid} \tag{11}$$

$$Y_E^* = -\left(y_{up} + y_{mid} + y_{mb} + \sum(a_j + 2b_j)y_j - y_{CO2,j} - y_{H2O,j} + y_{Si} + y_{Mn} + y_P + y_S + y_k\right) \tag{12}$$

The coordinates of the point R are given by Eq. (13) and Eq. (14), where D, E, F, ω_{OHC}, ω_{OC}, ω_{OH} and x_h are given by Eqs. (15)–(21).

$$Y_R = Y_A - r(Y_A - Y_W) \tag{13}$$

$$X_R = \frac{D(Y_R - Y_P) + (E+F)X_P}{Y_R - Y_P + E + F} \tag{14}$$

$$D = r\omega_{OHC} + 1 \tag{15}$$

$$E = r\omega_{OHC}\left(y_{up} + y_{mb}\right) \tag{16}$$

$$F = \left(y_{CO2,mid} + y_{H2O,mid} + y_{CO2,j} + y_{H2O,j} + y_e\right) \tag{17}$$

$$\omega_{OHC} = (1-x_h)\omega_{OC} + x_h\omega_{OH} \tag{18}$$

$$\omega_{OC} = 0.4089 + 3.8856\cdot10^{-3}T_R - 1.3778\cdot10^{-5}T_R^2 + 1.7924\cdot10^{-8}T_R^3 - 1.0465\cdot10^{-11}T_R^4 + 2.3054\cdot10^{-15}T_R^5 \tag{19}$$

$$\omega_{OH} = -0.0496 - 0.5075\cdot10^{-3}T_R + 0.4367\cdot10^{-5}T_R^2 - 0.6745\cdot10^{-8}T_R^3 + 0.4402\cdot10^{-11}T_R^4 - 1.0668\cdot10^{-15}T_R^5 \tag{20}$$

$$x_h = \frac{n_{H2} + n_{H2O}}{n_{CO} + n_{CO2} + n_{H2} + n_{H2O}} \tag{21}$$

The calculation of the extended operating line allows to compute the required mass flow of coke and air in the blast furnace (Eq. (22) and Eq. (23)).

$$m_K = n_{Fe}\frac{\mu + \frac{10^6\Omega_{HM,C}}{M_C n_{Fe}} - ey_v - \sum\left(\tau_j + a_j\right)y_j - y_{up} - y_{mid} - y_{mb}}{10^3\left(\frac{\Omega_{K,C}}{M_C} + \frac{\Omega_{K,H}}{M_{H2}}\right)} \tag{22}$$

$$m_{air} = \frac{y_v n_{Fe}\left(M_{O2} + \frac{0.79}{0.21}M_{N2}\right)}{2000(1 - \Omega_{air,H2O})} \tag{23}$$

The description of these terms can be found in the nomenclature list, and a detailed explanation of the methodology can be found in the work of Bailera et al. [33,37].

3.2. Aspen plus simulation

The extended operating line methodology was implemented in Aspen Plus to assess the 12 study cases. The model considers the upper, mid and lower zones of the blast furnace, with the latter zone including the raceways (Fig. 4). There are 10 inlet mass streams, three outlet mass

Table 3
Summary of model input/output data regarding the streams crossing the boundary of the blast furnace.

Stream	Description	Flow	Composition	Temperature
IR-OR-01	Iron ore	Input	Input	Input
COKE-01	Coke	Output	Input	Input
HB-01	Air + moisture	Output	Input	Input
COAL-01	Pulverized coal injection at tuyeres	Input	Input	Input
J-O2-01	O_2 injection for enrichment at tuyeres	Input	Input	Input
J-H2-01	H_2 injection at tuyeres	Input	Input	Input
J-RG-01	Gas injection at tuyeres	Input	Input	Input
TGR-01	Top gas recirculation injected at tuyeres	Input	Input	Input
M−INJ−01	Gas injection at mid shaft	Input	Input	Input
U-INJ-01	Gas injection at upper part	Input	Input	Input
HM-01	Hot metal	Output	Input	Input
SLAG-01	Slag	Output	Output	Input
BFG-01	Blast furnace gas	Output	Output	Output
HL-01	Heat removed by the staves	Input	–	–

streams and one outlet heat stream that cross the blast furnace boundary. The model computes the mass flow of coke, air, hot metal, slag and BFG, and the composition of the two latter, as a function of the temperature of the thermal reserve zone, the chemical efficiency, the heat removed by the staves in the preparation and in the elaboration zone, and the data specified as Input in Table 3.

The upper zone considers a stoichiometric reactor where the hematite is reduced to magnetite and wüstite. The inlets are the iron ore, the coke, the gas ascending from the thermal reserve zone, and (if present) a gas injection for preheating. The outlets are the blast furnace gas, and the solids descending to the mid zone. The extent of the iron ore reduction depends on the chemical efficiency, which sets the oxidation state of the burden descending to the mid zone. Moreover, the fraction of this reduction that takes place via H_2 is set according to the H_2 utilization, therefore calculating the outlet temperature of the BFG through the energy balance on the upper zone.

The mid zone consists of a stoichiometric reaction where the indirect reduction of magnetite to wüstite, and the reduction of wüstite to iron, take place. The inlets are the solids descending from the upper part, the gas ascending from the lower part, and (if exists) a reducing gas injection (shaft injection). The outlets are the gas ascending to the upper zone, and the solids descending to the lower zone. The extent of the reduction is set according to the percentage of indirect reduction calculated by the extended operating line methodology. The fraction of this reduction taking place via H_2 is set according to the chemical efficiency and the Chaudron diagram of the Fe—O—H system at the temperature of the thermal reserve zone.

The lower zone gathers five processes: the transfer of sulphur to the slag, the direct reduction of the remaining wüstite, the reduction of the accompanying elements, the carburization process, and the melting of slag and hot metal. The inlets to these processes are the solids descending from the mid zone, and the ashes and sulfur from the combustion of coal in the raceways. The outlets are the CO produced in these processes (which will be mixed with the raceways gas and sent to the mid zone), the remaining carbon after carburization (which is sent to the raceways at 1200 °C for combustion), and the final hot metal and slag.

The raceways consist of the decomposition of the coal through a Yield reactor, and the calculation of the chemical equilibrium of the combustion by a Gibbs reactor. The inlets are the injections of the auxiliary reducing agents, the air, and the coke carbon not consumed in other processes (at 1200 °C). The outlet is the raceway gas (whose temperature corresponds to the adiabatic flame temperature), and the sulphur and ashes (diverted to the processes of the lower zone). The raceway gas is mixed with the CO produced in the lower zone, and then sent to the mid zone.

The computer used for the simulation runs on 64-bit Windows 10 under a 11th Gen Intel® Core™ i7-1185G7 processor at 3.00 GHz, and 16 GB RAM. The discrepancy between the results of the extended operating line methodology (calculated in a Fortran subroutine) and the results obtained in the simulation is lower than 0.2 %. For further information on the different blocks and manipulators considered within the simulation, on the property methods, and on the property models, please see [33].

4. Results and discussion

4.1. Key performance indicators

In this study we compare 12 case studies using 7 KPIs. All the KPIs are analyzed as a function of KPI_1, which is the mass flow of syngas injected to the blast furnace. The graphs depicted in this section are for syngas injections within the range 0–200 kg/tHM.

4.1.1. KPI_2: Coke replacement ratio

The coke replacement ratio is the amount of coke that is saved in the blast furnace per kilogram of syngas injected (kg_{coke}/kg_{syngas}). In general, the highest replacement ratios were found in the oxygen blast furnace, while the lowest replacement ratios in the air-blown blast furnace, independently of the type of syngas (Table 4). This will have a direct implication on the potential decrease of CO_2 emissions when injecting syngas, which is expected to be lower in conventional blast furnaces. In addition, the replacement ratios were independent of the amount of syngas injected to the blast furnace.

The coke replacement ratio was in the range 0.13 – 0.16 kg_{coke}/kg_{syngas} when the syngas comes from biomass gasification (lower than the value found in literature, 0.3 kg_{coke}/kg_{syngas} [17]), around 0.12 – 0.19 kg_{coke}/kg_{syngas} when referred to plastic gasification (in agreement with literature, 0.18 kg_{coke}/kg_{syngas} [22]), from −0.05 to −0.08 kg_{coke}/kg_{syngas} for syngas from CO_2 electrolysis, and between 0.20 and 0.34 kg_{coke}/kg_{syngas} in the case of syngas produced by the RWGS reaction. Therefore, among the four types of syngas studied, the one produced through RWGS reaction showed replacement ratios 52 % – 113 % greater than the other types of syngas. The reason is because RWGS syngas has the higher volume fraction of reducing species (CO, H_2), and one of the lowers contents of oxidized species (CO_2, H_2O), compared to the other syngas. In fact, the syngas coming from CO_2 electrolysis has such a high CO_2 content that its replacement ratios are negative. The dissociation of this CO_2 in the raceways causes the available heat to drop so drastically that coke must be increased to fulfill the energy balance (i.e., injecting syngas from CO_2 electrolysis does not save coke, but increases its consumption).

Table 4
Coke replacement ratio by syngas injected at the tuyeres at 900 °C (kg_{coke}/kg_{syngas}).

Type of syngas	Air-blown blast furnace	Oxygen blast furnace	Advanced oxygen blast furnace
Biomass gasification	0.129	0.158	0.138
Plastic gasification	0.130	0.185	0.117
CO_2 electrolysis	−0.051	−0.082	−0.082
RWGS	0.198	0.337	0.230

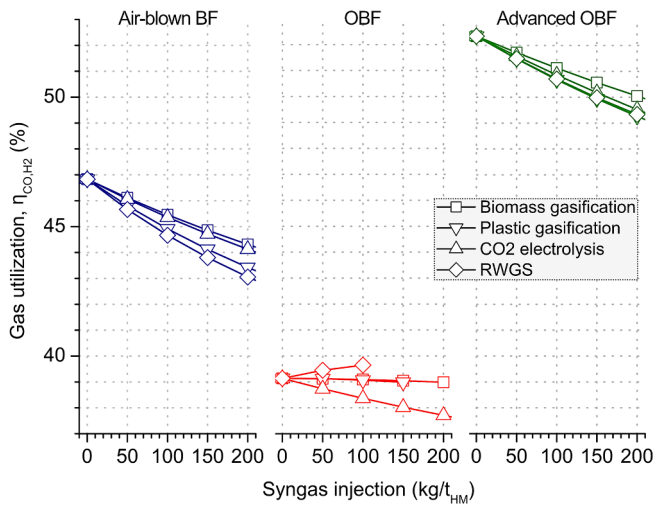

Fig. 5. Gas utilization, η_{CO,H_2}, (%) vs syngas injection (kg/tHM).

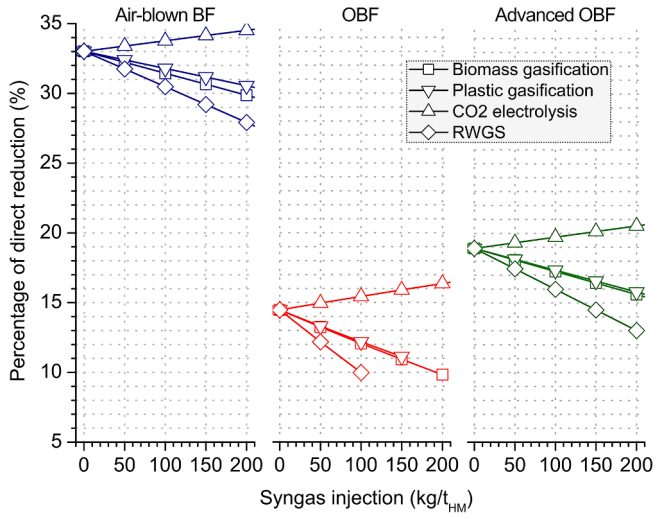

Fig. 6. Percentage of direct reduction (%) vs syngas injection (kg/tHM).

4.1.2. *KPI$_3$: Gas utilization*

The gas utilization is defined as the percentage of reducing species that are oxidized in the final blast furnace gas, i.e.,$\eta_{CO,H_2} = 100\cdot(n_{H2O}+n_{CO2})/(n_{CO}+n_{CO2}+n_{H2}+n_{H2O})$. This gives an idea on how much reducing gas was used in the blast furnace (although it should be kept in mind that some gas may had entered the blast furnace already oxidized). According to the model results, the gas utilization decreases by 0.012 – 0.018 pp/(kg_{syngas}/tHM) in air-blown blast furnaces, it varies between −0.007 and 0.005 pp/(kg_{syngas}/tHM) in oxygen blast furnaces, and drops 0.011 – 0.015 pp/(kg_{syngas}/tHM) in advanced oxygen blast furnaces (Fig. 5).

In OBF the overall gas utilization is much lower than in air-blown BF because the heat provided by the N_2 in the latter is now provided by recirculated CO in the OBF, leading to high CO contents in the blast furnace gas. In the case of advanced OBF, this heat is provided in the upper zone by an injection of CO_2 and H_2O, what remarkable rises the gas utilization.

4.1.3. *KPI$_4$: Percentage of direct reduction in the blast furnace*

The direct reduction is and endothermic reduction process that takes place in the lower part of the blast furnace (Eq. (24)). Since the injection of syngas provides less thermal energy than the fossil fuel it replaces, the

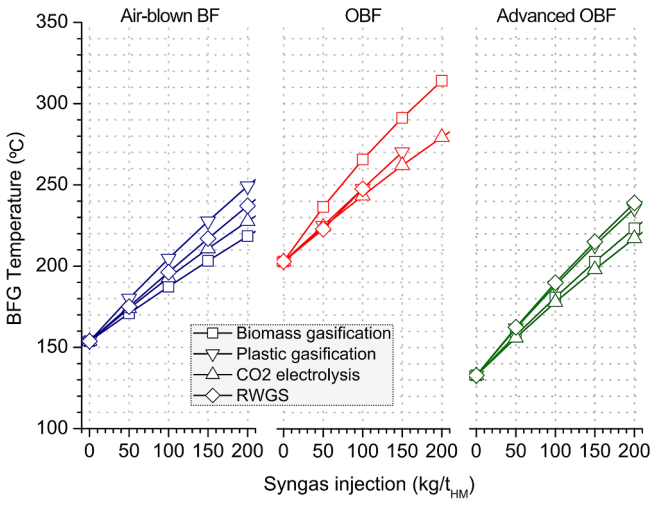

Fig. 7. Blast furnace gas temperature (°C) vs syngas injection (kg/tHM).

percentage of direct reduction must decrease to satisfy the energy balance (Fig. 6).

$$FeO + C \rightarrow Fe + CO \quad (24)$$

Nevertheless, it must be taken into account that the injection of CO_2 (and H_2O) at the tuyeres increases the amount of oxygen that is transferred via direct reduction from the iron oxides to the gas. This is because the direct reduction takes place as the combination of the dissociation of CO_2 (or H_2O) (Eq. (25)), plus the indirect reduction by CO (or by H_2) (Eq. (26)). The overall reaction is the direct reduction process (Eq. (27)), therefore injecting 1 mol of CO_2 (or H_2O) into de blast furnace implies transferring 1 mol of O from the iron oxides to the gas by direct reduction.

$$CO_2 + C \rightarrow 2CO \quad (25)$$

$$FeO + CO \rightarrow Fe + CO_2 \quad (26)$$

$$FeO + C \rightarrow Fe + CO \quad (27)$$

This effect is properly accounted in the extended operating line methodology, which showed in Fig. 6 that the higher the CO_2/H_2O content in the syngas, the less pronounce is the drop in the percentage of direct reduction (the CO/H_2 content of the syngas tends to increase the indirect reduction, but the CO_2/H_2O content palliates this effect). Furthermore, the percentage of direct reduction may even increase if the CO_2 content in the syngas is high enough to counterbalance the effect of the CO/H_2 content, like in the case of syngas from CO_2 electrolysis (Fig. 6). It should be noted that the conventional Rist diagram does not take this into account, so it overestimates the drop in the percentage of direct reduction.

In air-blown blast furnaces, the percentage of direct reduction varies −0.026 – 0.007 pp/(kg_{syngas}/tHM), in oxygen blast furnaces −0.045 – 0.009 pp/(kg_{syngas}/tHM), and in advanced oxygen blast furnaces −0.029 – 0.008 pp/(kg_{syngas}/tHM). In general, the percentage of direct reduction decreases with syngas injection more significantly for OBF than for BF and AdOBF. In practice, the percentage of direct reduction should not fall below 5 % (technical limitation according to [39]), but none of the studied configurations reach this limit, mainly because of accounting for the direct reduction associated to the dissociation of CO_2 and H_2O. Actually, the operating points of OBF with 150 and 200 kg/tHM of syngas injection from RWGS, and the operating point of 200 kg/tHM of syngas injection from plastic gasification, cannot meet the energy balance since they would require percentages of direct reduction below the value that the injection itself already implies.

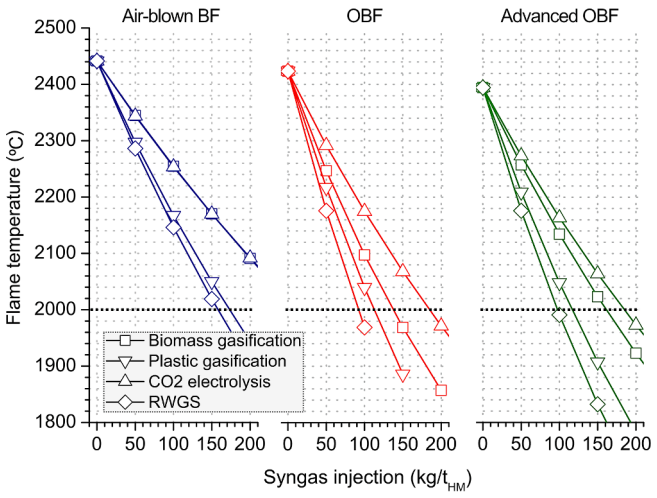

Fig. 8. Flame temperature (°C) vs syngas injection (kg/tHM).

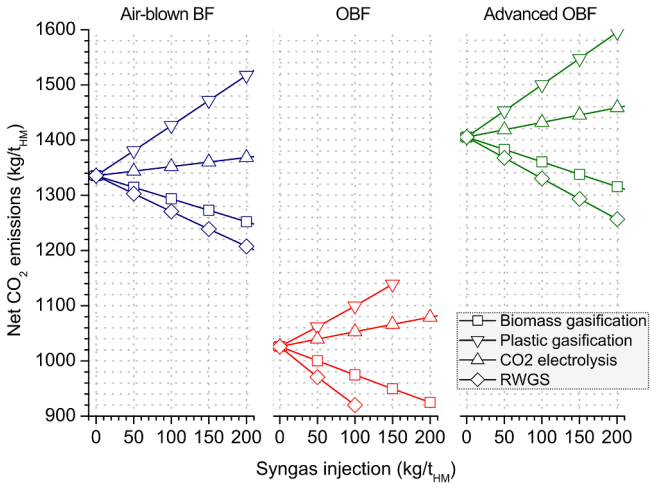

Fig. 9. Net CO_2 emissions (kg/tHM) vs syngas injection (kg/tHM).

4.1.4. KPI_5: BFG temperature

The temperature of the blast furnace gas is calculated through an energy balance on the upper zone of the blast furnace [37]. The assumptions taken in this balance (H_2 utilization and heat removed by the staves) influence the behavior of BFG temperature. In summary, the larger the syngas injection, the greater the heat available in the upper zone of the blast furnace, and the higher the BFG temperature must be to fulfill the energy balance. The three main reasons for which there is more thermal energy available are: (i) the increment of the H_2 mole flow in the gas (its specific heat is greater than for the other components); (ii) the increase of the BFG mass flow; and (iii) the decrease of the coke mass flow. In (i) and (ii), there is more sensible heat available from the gases, therefore the final temperature of the BFG must increase to satisfy the energy balance because the cooling of the staves is fixed. In (iii), the heating of the solids entering at the top requires less energy, what translates again into more available energy in the gases. In air-blown blast furnaces, the BFG temperature increases 0.31 – 0.45 °C/(kg_{syngas}/tHM), in oxygen blast furnaces 0.37 – 0.55 °C/(kg_{syngas}/tHM), and in advanced oxygen blast furnaces 0.40 – 0.53 °C/(kg_{syngas}/tHM). In general, results showed that the increment in the BFG temperature is smaller in air-blown BF than in OBF and AdOBF (Fig. 7). It should be noted that the BFG temperature should not be lower than 100 °C in order to avoid corrosion problems (water condensation) or higher than 300 °C in order to avoid damaging the feeding system at the top of the BF.

4.1.5. KPI_6: Flame temperature

The flame temperature decreases when injecting syngas because of the lower thermal energy provided in comparison with the combustion of the replaced coke. In air-blown blast furnaces, the flame temperature drops by 1.6 – 2.5 °C/(kg_{syngas}/tHM), in oxygen blast furnaces decreases 2.1 to 4.5 °C/(kg_{syngas}/tHM), and in advanced oxygen blast furnaces between 1.9 and 3.5 °C/(kg_{syngas}/tHM). Like for the BFG temperature, the less pronounced variations are found in the air-blown blast furnace. When comparing the different syngas, the results showed that the higher the hydrogen content (whether as H_2 or as CH_4) the steeper the drop in temperature (Fig. 8). In general, these values are of the same order of magnitude that the decrease in the flame temperature stated in literature for coke replacements by methane injection, 4.5 °C/(kg_{CH4}/tHM) [6]. This KPI is one of the most important parameters when assessing new operating conditions, since 2000 °C is generally considered in literature as the minimum reasonable technical limit [7]. Nevertheless, according to Babich [39], some blast furnaces have been successfully operated with 1600 – 1700 °C flame temperatures (the lower the percentage of direct reduction, the lower the minimum limit for the flame temperature can be).

4.1.6. KPI_7: Net CO_2 emissions

The net CO_2 emissions are computed as the total CO_2-equivalent emissions exiting the system (i.e., the CO_2-equivalent from the BFG not recirculated, plus the CO_2 from amine scrubbing) minus the contribution of the syngas injection (except for plastic-based syngas). These are directly related with the coke replacement ratio (Table 4), since the higher the amount of coke replaced, the higher the CO_2 avoided. The net CO_2 emissions (Fig. 9) also follows the trend of the percentage of direct

Table 5
Mass flows (kg/tHM) and composition of BFG for the air-blown blast furnace under the base case (no injection of syngas), and under the maximum possible injection of syngas that keeps the flame temperature at 2000 °C.

Mass flow (kg/tHM)	Air-blown blast furnace	Air-blown blast furnace with injection of syngas from:			
		biomass gasification	plastic gasification	CO_2 electrolysis	RWGS
Iron ore	1558	1558	1558	1558	1558
Coke	288	255	266	301	257
Pulverized coal	200	200	200	200	200
Syngas (at tuyeres)	–	261	173	264	158
Hot blast (27 vol% O_2)	1147	1046	1151	1182	1056
Hot metal	1002	1002	1002	1002	1002
Slag	262	258	259	263	258
BFG	1930	2060	2087	2241	1969
CO (%vol.)	24.3	25.1	24.7	29.4	23.1
CO_2 (%vol.)	23.4	22.5	22.2	23.9	21.9
H_2 (%vol.)	4.6	9.2	8.9	4.0	12.1
H_2O (%vol.)	2.1	4.1	4.0	1.8	5.4
N_2 (%vol.)	45.6	39.1	40.2	40.9	37.5

reduction (Fig. 6), because the direct reduction implies the consumption of coke carbon (Eq. (24)), and therefore more emissions. Thus, the higher the content of reducing species (CO, and especially H_2) and the lower the content of oxidized species (CO_2, H_2O) in the syngas, the lower the net CO_2 emissions.

In air-blown blast furnaces, the net CO_2 emissions may decrease 0.42 – 0.63 $kg_{CO2\text{-}eq}/kg_{syngas}$, in oxygen blast furnaces by 0.50 to 1.06 $kg_{CO2\text{-}eq}/kg_{syngas}$, and in advanced oxygen blast furnaces between 0.38 and 0.74 $kg_{CO2\text{-}eq}/kg_{syngas}$. However, emissions will increase by 0.16 – 0.27 $kg_{CO2\text{-}eq}/kg_{syngas}$ if syngas from CO_2 electrolysis is used (because of its negative coke replacement ratios), and by 0.75 – 0.95 $kg_{CO2\text{-}eq}/kg_{syngas}$ if syngas from plastic gasification is used (since this syngas is not considered CO_2-neutral). It can be concluded that the oxygen blast furnace configuration has the best potential to reduce CO_2 emissions when injecting syngas. Furthermore, thanks to the carbon capture stage (Fig. 2), about 50 % of the emitted CO_2 in OBF is pure and available for underground storage. In addition, it presents the lower net CO_2 emissions even at no syngas injection, mainly because of the high amount of reducing gas recirculated from the BFG that is injected at the shaft and tuyeres.

4.2. Comparing the limits of injection of the different syngas

According to the limitation on the flame temperature (≥2000 °C), the maximum amount of syngas that can be injected will depend on the BF configuration and the type of syngas (Fig. 8). The results of the Aspen Plus simulation for each of the 12 study cases, as well as the base cases, are presented in Table 5, Table 6 and Table 7 for this limiting operating point. In air-blown blast furnaces, the maximum injection of syngas is in the range 158–264 kg_{syngas}/tHM, in oxygen blast furnaces between 92 and 185 kg_{syngas}/tHM, and in advanced oxygen blast furnaces in the span from 97 to 185 kg_{syngas}/tHM. The upper limits correspond to syngas from CO_2 electrolysis, and the lower limits to syngas from RWGS reaction, because the higher the ratio H:C in the syngas, the faster the flame temperature drops.

Nevertheless, it should be noted that greater syngas injections do not necessarily imply higher reductions of the CO_2 emissions (Table 8). Actually, the highest decrease on CO_2 emissions (as well as the lowest CO_2 emissions) is achieved with syngas from RWGS reaction in oxygen blast furnaces, whose injection is limited to 92 kg_{syngas}/tHM (the lowest limit of all study cases). Furthermore, maximizing the amount of emitted CO_2 that comes from the syngas (i.e., that is neutral) neither guarantees maximizing the decrease in the final net emissions. For example, the configurations using syngas from CO_2 electrolysis may have shares of neutral CO_2 of up to 20 %, but they still lead to the highest net CO_2 emissions. At the end, the most important factor to reduce CO_2 emissions is to increase the ratio H:C of the syngas.

Since the injection of syngas from RWGS provides the highest CO_2 emission reduction with the lowest syngas mass flow injections, the extended operating lines for these configurations have been depicted in Fig. 10. Since the right side of the diagram depicts the moles of oxygen transferred from the iron oxides to the gas by indirect reduction (instead of the oxidation state of the gas as in the conventional Rist diagram), the axis of the phase diagrams must be transformed to have a correct

Table 6
Mass flows (kg/tHM) and composition of BFG for the oxygen blast furnace under the base case (no injection of syngas), and under the maximum possible injection of syngas that keeps the flame temperature at 2000 °C.

Mass flow (kg/tHM)	Oxygen blast furnace	Oxygen blast furnace with injection of syngas from:			
		biomass gasification	plastic gasification	CO_2 electrolysis	RWGS
Iron ore	1558	1558	1558	1558	1558
Coke	219	197	199	234	189
Pulverized coal	170	170	170	170	170
Syngas (at tuyeres)	–	137	112	185	92
Hot blast (99 vol% O_2)	302	289	300	313	282
Tuyere recirculation	308	311	274	315	255
Shaft recirculation	463	467	411	473	382
Hot metal	1002	1001	1001	1002	1001
Slag	251	249	249	253	248
BFG	1768	1881	1775	1995	1679
CO (%vol.)	49.8	42.6	44.4	53.7	40.0
CO_2 (%vol.)	34.0	30.0	31.5	33.9	30.3
H_2 (%vol.)	9.9	14.1	15.7	7.7	19.5
H_2O (%vol.)	4.4	6.3	7.1	3.5	8.8
N_2 (%vol.)	1.9	7.0	1.3	1.2	1.4

Table 7
Mass flows (kg/tHM) and composition of BFG for the advanced oxygen blast furnace under the base case (no injection of syngas), and under the maximum possible injection of syngas that keeps the flame temperature at 2000 °C.

Mass flow (kg/tHM)	Advanced oxygen blast furnace	Advanced oxygen blast furnace with injection of syngas from:			
		biomass gasification	plastic gasification	CO_2 electrolysis	RWGS
Iron ore	1558	1558	1558	1558	1558
Coke	246	224	233	261	224
Pulverized coal	200	200	200	200	200
Syngas (at tuyeres)	–	162	116	185	97
Methane (at tuyeres)	75	75	75	75	75
Hot blast (99 vol% O_2)	422	405	425	434	406
Upper injection	328	314	316	331	308
Hot metal	1002	1002	1002	1002	1002
Slag	257	255	256	259	255
BFG	1565	1682	1666	1784	1612
CO (%vol.)	35.5	35.4	36.1	39.6	34.5
CO_2 (%vol.)	34.2	29.8	30.4	33.8	28.8
H_2 (%vol.)	11.9	12.9	13.1	10.4	14.5
H_2O (%vol.)	17.8	19.3	19.7	15.6	21.7
N_2 (%vol.)	0.6	2.5	0.5	0.5	0.5

Table 8
CO_2-equivalent emissions for the 12 study cases under the maximum possible injection of syngas (i.e., flame temperature at 2000 °C).

Blast furnace	Syngas from	Total CO_2 emissions (kg/tHM)	CO_2 emissions from syngas (%)	CO_2 emissions from fossil fuel (%)	Net CO_2 emissions (kg/tHM)	CO_2 emissions reduction (%)
Air-blown BF	–	1336	–	100	1336	–
Air-blown BF	Biomass	1499	18.1	81.9	1227	8.1
Air-blown BF	Plastic	1493	15.4	84.6	1493	−11.7
Air-blown BF	CO_2 electrolysis	1717	19.7	80.3	1379	−3.2
Air-blown BF	RWGS	1402	12.0	88.0	1234	7.6
OBF	–	1026	–	100	1026	–
OBF	Biomass	1099	13.0	87.0	956	6.8
OBF	Plastic	1109	13.4	86.6	1109	−8.1
OBF	CO_2 electrolysis	1312	18.0	82.0	1075	−4.8
OBF	RWGS	1025	9.5	90.5	928	9.5
Advanced OBF	–	1405	–	100	1405	–
Advanced OBF	Biomass	1500	11.2	88.8	1332	5.2
Advanced OBF	Plastic	1515	10.2	89.8	1515	−7.8
Advanced OBF	CO_2 electrolysis	1691	14.0	86.0	1454	−3.5
Advanced OBF	RWGS	1436	7.2	92.8	1332	5.2

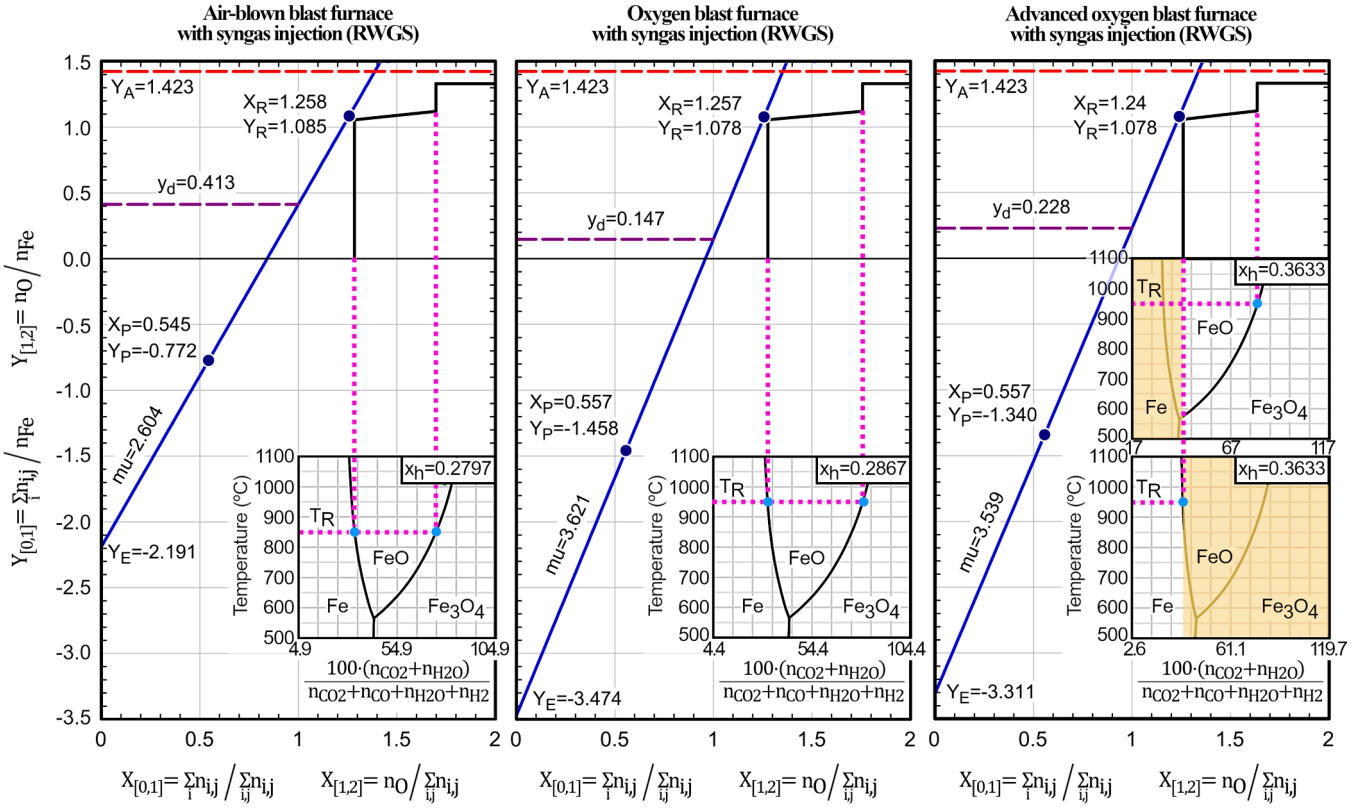

Fig. 10. Extended operating lines for air-blown blast furnace, oxygen blast furnace, and advanced oxygen blast furnace, under the maximum possible injection of syngas from RWGS (i.e., flame temperature at 2000 °C).

comparison. Moreover, in the case of advances oxygen blast furnaces, where an upper injection exists, the phase diagram changes from that point onwards because the oxidation state of the gas is modified on a non-continuous way (these kind of effects cannot be taken into account with the conventional Rist diagram).

5. Conclusions

This paper analyzed and compared the injection of different syngas in air-blown blast furnaces, oxygen blast furnaces, and advanced oxygen blast furnaces. The selected types of syngas were syngas from biomass gasification, syngas from waste plastic gasification, syngas from CO_2 electrolysis, and syngas from the reverse water–gas shift reaction. An Aspen Plus model, based on the new extended operating line methodology, was used for the simulation [33]. This methodology is a generalization of the conventional Rist diagram, to extend its application to cases in which the injected gases have large contents of CO_2 and H_2O, and also to cases in which injections take place at the middle or upper zone of the blast furnace. The base cases were elaborated and validated with data from literature, with a discrepancy below 3.5 %.

To assess the 12 scenarios (4 types of syngas × 3 types of blast furnace), 7 key performance indicators were defined (mass flow of syngas, coke replacement ratio, gas utilization, percentage of direct reduction, BFG temperature, flame temperature, and net CO_2

emissions). The highest replacement ratios were found in the oxygen blast furnace (0.16 – 0.34 kg_{coke}/kg_{syngas}), where the greatest value corresponds to syngas from RWGS. The gas utilization, defined as the percentage of reducing species that are oxidized in the final blast furnace gas, decreases in most cases. The lowest drops are found in the oxygen blast furnaces ($\leq$0.005 pp/(kg_{syngas}/tHM)) because this configuration recirculates a large amount of CO into the shaft and tuyeres, making any variation less relevant. Regarding the percentage of direct reduction, the higher the CO_2/H_2O injection rates, the smaller the drop in the percentage of direct reduction. This drop can even turn negative (i.e., to lead to increments in the direct reduction) if the CO_2 injection rate is high enough, like in the case of syngas from CO_2 electrolysis. Nevertheless, in none of the 12 study cases the percentage of direct reduction falls below 5 %, which is considered a technical limit. The temperature of the BFG increases in all cases, between 0.31 and 0.55 °C/(kg_{syngas}/tHM). In general, results showed that this increment is lower in air-blown BF than in OBF and AdOBF. The flame temperature drops by 1.6 – 4.5 °C/(kg_{syngas}/tHM) because of syngas injections, with the decrease being steeper at higher H:C ratios. The net CO_2 emissions were found to be directly related with the coke replacement ratio, therefore the highest cuts can be reached in OBF (0.50 to 1.06 $kg_{CO2\text{-}eq}/kg_{syngas}$).

In practice, the amount of syngas that can be injected is limited by the drop in the flame temperature. Considering the 12 study cases, the maximum syngas injection varies between 92 and 264 kg_{syngas}/tHM. Nevertheless, greater syngas injections do not necessarily imply higher reductions of the CO_2 emissions. Actually, the lowest net CO_2 emissions are achieved with syngas from RWGS reaction in OBF, whose injection limit is 92 kg_{syngas}/tHM. The reason is the high H:C ratio of this syngas. Under this configuration, the OBF emits 1025 $kg_{CO2\text{-}eq}$/tHM, of which 9.5 % are neutral CO_2 emissions because they originally come from the syngas (i.e., the net CO_2 emissions are 928 $kg_{CO2\text{-}eq}$/tHM).

CRediT authorship contribution statement

Manuel Bailera: Conceptualization, Methodology, Software, Validation, Formal analysis, Investigation, Writing – original draft, Visualization, Funding acquisition.

Declaration of Competing Interest

The authors declare that they have no known competing financial interests or personal relationships that could have appeared to influence the work reported in this paper.

Data availability

Data will be made available on request.

Acknowledgements

This project has received funding from the European Union's Framework Programme for Research and Innovation Horizon 2020 (2014-2020) under the Marie Skłodowska-Curie Grant Agreement No. 887077.

References

[1] International Energy Agency. Iron and Steel Technology Roadmap. 2020.
[2] Quader MA, Ahmed S, Ghazilla RAR, Ahmed S, Dahari M. A comprehensive review on energy efficient CO2 breakthrough technologies for sustainable green iron and steel manufacturing. Renew Sustain Energy Rev 2015;50:594–614. https://doi.org/10.1016/j.rser.2015.05.026.
[3] De Ras K, Van de Vijver R, Galvita VV, Marin GB, Van Geem KM. Carbon capture and utilization in the steel industry: challenges and opportunities for chemical engineering. Curr Opin Chem Eng 2019;26:81–7. https://doi.org/10.1016/j.coche.2019.09.001.
[4] Fenton MD, Tuck CA. Iron and Steel. 2016 Minerals Yearbook. US Geological Survey. 2019.
[5] Wang Q, Zhu Y, Wu Q, Gratz E, Wang Y. Low temperature electrolysis for iron production via conductive colloidal electrode. RSC Adv 2015;5:5501–7. https://doi.org/10.1039/C4RA14576C.
[6] Babich A, Senk D, Gudenau H, Mavrommatis KT. Ironmaking Textbook. RWTH Aachen University; 2008.
[7] Geerdes M, Chaigneau R, Lingiardi O, Molenaar R van O, R. SY, Warren J. Modern Blast Furnace Ironmaking An Introduction. IOS Press; 2020.
[8] Ueckerdt F, Bauer C, Dirnaichner A, Everall J, Sacchi R, Luderer G. Potential and risks of hydrogen-based e-fuels in climate change mitigation. Nat Clim Chang 2021;11:384–93. https://doi.org/10.1038/s41558-021-01032-7.
[9] Mac Dowell N, Fennell PS, Shah N, Maitland GC. The role of CO2 capture and utilization in mitigating climate change. Nat Clim Chang 2017;7:243–9. https://doi.org/10.1038/nclimate3231.
[10] Perpiñán J, Bailera M, Romeo LM, Peña B, Eveloy V. CO2 Recycling in the Iron and Steel Industry via Power to Gas and Oxy-Fuel Combustion. Energies 2021;14:7090. https://doi.org/10.3390/en14217090.
[11] Bailera M, Lisbona P, Pérez V. Syngas utilization in the iron and steel industry. Advances in Synthesis Gas: Methods. Technologies and Applications Syngas Products and Usages, Elsevier 2022. https://doi.org/10.1016/B978-0-323-91878-7.00002-2.
[12] Pérez V, Bailera M, Lisbona P. Syngas production by gasification processes. Advances in Synthesis Gas: Methods, Technologies and Applications. Syngas Production and Preparation: Elsevier; 2022. https://doi.org/10.1016/B978-0-323-91871-8.00020-9.
[13] Wiklund CM, Helle M, Saxén H. Economic assessment of options for biomass pretreatment and use in the blast furnace. Biomass Bioenergy 2016;91:259–70. https://doi.org/10.1016/j.biombioe.2016.05.033.
[14] Wang C, Mellin P, Lövgren J, Nilsson L, Yang W, Salman H, et al. Biomass as blast furnace injectant - Considering availability, pretreatment and deployment in the Swedish steel industry. Energy Convers Manag 2015;102:217–26. https://doi.org/10.1016/j.enconman.2015.04.013.
[15] Wang C, Larsson M, Lövgren J, Nilsson L, Mellin P, Yang W, et al. Injection of solid biomass products into the blast furnace and its potential effects on an integrated steel plant. Energy Procedia 2014;61:2184–7. https://doi.org/10.1016/j.egypro.2014.12.105.
[16] Liu Y, Shen Y. Modelling and optimisation of biomass injection in ironmaking blast furnaces. Prog Energy Combust Sci 2021;87:100952. https://doi.org/10.1016/j.pecs.2021.100952.
[17] Babich A, Senk D, Solar J, de Marco I. Efficiency of biomass use for blast furnace injection. ISIJ Int 2019;59:2212–9. https://doi.org/10.2355/isijinternational.ISIJINT-2019-337.
[18] Hayashi K, Kasahara S, Kuribara K, Nakagaki T, Yan XL, Inagaki Y, et al. Process evaluation of use of high temperature gas-cooled reactors to an ironmaking system based on active carbon recycling energy system. ISIJ Int 2015;55(2):348–58. https://doi.org/10.2355/isijinternational.55.348.
[19] Nomura S. Blast furnace feedstock and coke oven chemical feedstock. Elsevier Inc.; 2020. doi: 10.1016/b978-0-12-817880-5.00012-8.
[20] Devasahayam S. Review: Opportunities for simultaneous energy/materials conversion of carbon dioxide and plastics in metallurgical processes. Sustain Mater Technol 2019;22:e00119. https://doi.org/10.1016/j.susmat.2019.e00119.
[21] Ariyama T. Transition of waste plastics utilization in blast furnace and future aspect. Nihon Enerugi Gakkaishi/Journal Japan Inst Energy 2010;89:528–36.
[22] Rieger J, Colla V, Matino I, Branca TA, Stubbe G, Panizza A, et al. Residue Valorization in the Iron and Steel Industries: Sustainable Solutions for a Cleaner and More Competitive Future Europe. Metals (Basel) 2021;11(8). https://doi.org/10.3390/met11081202.
[23] Bailera M, Lisbona P, Romeo LM, Espatolero S. Power to Gas projects review: Lab, pilot and demo plants for storing renewable energy and CO2. Renew Sustain Energy Rev 2017;69:292–312. https://doi.org/10.1016/j.rser.2016.11.130.
[24] Strohbach O. Audi e-gas plant stabilizes electrical grid. Press Release - Audi MediaInfo - Technol Innov Commun 2015.
[25] Bailera M, Hanak DP, Lisbona P, Romeo LM. Techno-economic feasibility of power to gas–oxy-fuel boiler hybrid system under uncertainty. Int J Hydrogen Energy 2019;44(19):9505–16. https://doi.org/10.1016/j.ijhydene.2018.09.131.
[26] Kuparinen K. Transforming the chemical pulp industry - From an emitter to a source of negative CO2 emissions. LUT University Press; 2019..
[27] Bailera M, Espatolero S, Lisbona P, Romeo LM. Power to gas-electrochemical industry hybrid systems: A case study. Appl Energy 2017;202:435–46. https://doi.org/10.1016/j.apenergy.2017.05.177.
[28] Kato Y. Carbon recycling for reduction of carbon dioxide emission from iron-Making process. ISIJ Int 2010;50:181–5. https://doi.org/10.2355/isijinternational.50.181.
[29] Bailera M, Lisbona P, Peña B, Romeo LM. A review on CO2 mitigation in the Iron and Steel industry through Power to X processes. J CO2 Util 2021;46. https://doi.org/10.1016/j.jcou.2021.101456.
[30] Kato Y. Utilization of HTGR on active carbon recycling energy system. Nucl Eng Des 2014;271:79–83. https://doi.org/10.1016/j.nucengdes.2013.11.014.
[31] Jin P, Jiang Z, Bao C, Lu Y, Zhang J, Zhang X. Mathematical Modeling of the Energy Consumption and Carbon Emission for the Oxygen Blast Furnace with Top Gas Recycling. Steel Res Int 2016;87:320–9. https://doi.org/10.1002/srin.201500054.
[32] Sato M, Takahashi K, Nouchi T, Ariyama T. Predictcion of next-generation ironmaking process based on oxygen blast furnace suitable for CO2 mitigation and energy flexibility. ISIJ Int 2015;55:2105–14. https://doi.org/10.2355/isijinternational.ISIJINT-2015-264.

[33] Bailera M, Nakagaki T, Kataoka R. Extending the operating line methodology to consider shaft and preheating injections in blast furnaces. ISIJ Int 2022;62. https://doi.org/10.2355/isijinternational.ISIJINT-2022-111.
[34] Salaudeen SA, Arku P, Dutta A. Gasification of plastic solid waste and competitive technologies. Elsevier Inc.; 2018. doi: 10.1016/B978-0-12-813140-4.00010-8.
[35] Sahu RK, Roy SK, Sen PK. Applicability of Top Gas Recycle Blast Furnace with Downstream Integration and Sequestration in an Integrated Steel Plant. Steel Res Int 2015;86:502–16. https://doi.org/10.1002/srin.201400196.
[36] Rist A, Meysson N. A dual graphic representation of the blast-furnace mass and heat balances. Jom 1967;19:50–9. https://doi.org/10.1007/bf03378564.
[37] Bailera M, Nakagaki T, Kataoka R. Revisiting the Rist diagram for predicting operating conditions in blast furnaces with multiple injections. Open Res Eur 2021; 1. https://doi.org/10.12688/openreseurope.14275.1.
[38] Meysson N, Weber J, Rist A. Représentation graphique de la décomposition des carbonates dans le haut fourneau. Rev Métallurgie 1964;61:623–33. https://doi.org/10.1051/metal/196461070623.
[39] Babich A. Blast furnace injection for minimizing the coke rate and CO2 emissions. Ironmak Steelmak 2021;48:728–41. https://doi.org/10.1080/03019233.2021.1900037.